

PERMEABILITIES OF SEDIMENTS FROM WOODLARK BASIN: IMPLICATIONS FOR PORE PRESSURES¹

Amy Kemerer² and Elizabeth Screaton²

ABSTRACT

Woodlark Basin, an area of continental extension, is an ideal location to study the evolution of permeability and the development of overpressures within an active rift basin. In this investigation, we measured sediment permeabilities of cores from Woodlark Basin and used numerical modeling to determine if pore fluid overpressures are likely at the base of the rift basin. Constant-rate flow tests were conducted on cores from Site 1108, located in the rift basin, and Sites 1115 and 1118, located on the northern margin of the basin. Results of the laboratory tests indicated permeabilities that range from 1.5×10^{-18} to 1×10^{-16} m². Results of the numerical modeling of Site 1108 suggest that overpressures due to sedimentation are unlikely.

INTRODUCTION

Sedimentary basins are the settings for many interrelated geologic processes such as fluid flow, heat flow, solute transport, and rock-water interactions (Person et al., 1996). Mature sedimentary basins, such as the Gulf of Mexico basin and the North Sea, are the sites for many of the world's most valuable petroleum and natural gas reservoirs (Mello and Karner, 1996). Active and ancient rift basins contain many important metal ore deposits (Person and Garven, 1994). Fluid flow plays a vital role in geochemical, geothermal, and tectonic processes within sedimentary basins and can assist in the generation of cements and ore deposits, as well as in the migration of petroleum hydrocarbons (Person

¹Kemerer, A., and Screaton, E., 2001. Permeabilities of sediments from Woodlark Basin: implications for pore pressures. In Huchon, P., Taylor, B., and Klaus, A. (Eds.), *Proc. ODP, Sci. Results*, 180, 1–14 [Online]. Available from World Wide Web: <http://www-odp.tamu.edu/publications/180_SR/VOLUME/CHAPTERS/169.PDF>. [Cited YYYY-MM-DD]
²Department of Geological Sciences, University of Florida, 241 Williamson, Box 112120, Gainesville FL 32611, USA. Correspondence author: screaton@geology.ufl.edu

and Garven, 1994). In addition, fluid pressures have been suggested to play a role in fault mechanics (Hubbert and Rubey, 1959; Axen, 1992; Rice, 1992).

An important mechanism for generating overpressures is sediment loading (Bethke, 1985; Bredehoeft et al., 1988; Mello and Karner, 1996). In sedimentary basins, sediment is rapidly being added to the basin floor. The new sediment adds additional load to the older sediments beneath and increases fluid pressures. Elevated fluid pressures drive fluid flow, and as fluid escapes, the stress between the individual grains of the sediment (effective stress) is increased, bulk volume is reduced, and porosity is lost.

If permeability is sufficiently low, the pore fluids will be unable to escape at a rate comparable to the rate of loading due to sedimentation. When this occurs, the pore fluid pressure will increase above hydrostatic, a condition termed overpressuring, geopressing, or excess pressuring (Osborne and Swarbrick, 1997; Bjørlykke and Hoeg, 1997; Mello and Karner, 1996).

Because permeabilities control the compaction of sediment, development of overpressures, and patterns of fluid flow, this parameter plays a key role in sedimentary basin evolution. Elevated pore pressures have also been suggested to facilitate low-angle normal faulting (Axen, 1992). Ocean Drilling Program (ODP) Leg 180 investigated processes associated with active rifting in the Woodlark Basin. Samples from ODP Leg 180 were used in this investigation to determine vertical permeabilities within sediments of the Woodlark Basin, as well as the relationship between basin sedimentation and elevated pore fluid pressures. A constant flow permeability test was performed on each sample to determine permeability. These values were then incorporated into a numerical model to quantify the relationship between sediment permeability, basin sedimentation rates, and the development of pore fluid overpressures.

BACKGROUND

Woodlark Basin, located between the easternmost Papuan Peninsula and the Solomon Islands in the South Pacific, is a young ocean basin that has been forming since 6 Ma, as a result of a westward propagating spreading center. The spreading center has stretched and separated the eastern Papuan Peninsula from its eastern paleoextensions, the Woodlark and Pocklington Rises (Taylor et al., 1995). According to Mobbs (1997), spreading in the basin initiated sometime prior to 3.5 Ma. A significant feature of Woodlark Basin is Moresby Seamount, located just south and west of the spreading tip (Fig. F1). Moresby Seamount forms the footwall of a low-angle normal fault that dips 25°–30° beneath a 3.2-km-deep rift basin (Shipboard Scientific Party, 1999).

During Leg 180, three sites (1109, 1115, and 1118) on the northern margin of the basin were cored to depths of 802, 803, and 927 meters below seafloor (mbsf), respectively (Fig. F1). All three sites (1109, 1115, and 1118) show evidence of subsidence from shallow-marine to deeper bathyal water conditions (Shipboard Scientific Party, 1999). This transition probably began in the latest Miocene to early Pliocene and occurred first at Site 1109 then at Sites 1115 and 1118. The sediments from these sites were distally derived and contain variable volcanogenic input. Sediments on the northern margin are only slightly deformed and can be dated and correlated well. Site 1108 was drilled above the

F1. Location of Sites 1108, 1109, 1115, and 1118 relative to Moresby Seamount, p. 12.



low-angle fault zone emerging north of Moresby Seamount. One objective of Leg 180 was to measure pore pressures and stresses within and surrounding this low-angle fault zone. The presence of hydrocarbons and drilling difficulties limited coring at Site 1108 to a depth of only 485 mbsf, short of the low-angle fault (~900 mbsf).

Recorded sedimentation at Site 1108 includes rapid deposition of fine-, medium-, and coarse-grained sandstones, terrigenous turbidites, and minor conglomerates (Shipboard Scientific Party, 1999). These deposits are overlain by fine-grained turbidites and talus deposits. In the late Pleistocene, sediments consisted of calcareous nannofossil-rich clay with minor silt and sand, including volcanic ash, and apparent deposition rates are low (15 m/m.y.). However, shipboard porosity data and postcruise consolidation testing suggested that ~400 m of sediment has been removed from Site 1108 by a combination of erosion and normal faulting (Shipboard Scientific Party, 1999; Bolton et al., 2000). Leg 180 drilling at other sites suggests that upper levels of the basement of Moresby Seamount are primarily dolerite (Shipboard Scientific Party, 1999).

METHODS

Constant Flow Permeability Tests

Constant flow permeability tests were conducted to determine vertical permeability values for core samples from Leg 180. In this test method, a constant flow is established across the sample and the resulting hydraulic gradient is measured. The tests were conducted using the Trautwein Soil Testing Equipment Company's DigiFlow K. The equipment consists of the cell (to contain the sample and the confining fluid) and three pumps (sample top pump, sample bottom pump, and cell pump). Bladder accumulators allowed deionized water to be used throughout the pumps while an idealized solution of seawater (25 g NaCl and 8 g MgSO₄ per liter of water) was used as the permeant through the sample. ASTM designation D 5084-90 (1990) was used as a guideline for general procedures. The Leg 180 whole-round samples were stored in the plastic core liner and sealed in wax to prevent moisture loss. They were contained in a refrigerated environment (4°C) and in water until immediately prior to sample preparation. Immediately before testing, cores were trimmed to fit within the flexible wall membrane. The samples had a minimum diameter of 50.8 mm (2 in), and sample heights ranged from ~150 to 200 mm. The ends of each sample were trimmed to provide freshly exposed surfaces. Once encased within the flexible wall membrane, the samples were fitted with filter paper and saturated porous disks. Samples were placed in the cell, which was then filled with deionized water so that the membrane-encased sample was completely surrounded by this fluid. A small confining pressure of ~0.03 MPa (5 psi) was applied to the cell. All air bubbles were removed from the flow lines, and a backpressure of ~0.28 MPa (40 psi) was then applied in order to fully saturate the sample. Backpressure was achieved by concurrently ramping the cell pressure and the sample pressure to maintain a steady effective stress. Saturation was verified by measuring the change in pore water pressure in the porous material divided by the change in the confining pressure (ASTM, 1990).

Once the sample was fully saturated, cell fluid pressure was increased while the sample backpressure was maintained, thus increasing the ef-

fective stress on the sample. The maximum stress that the cell is able to sustain is ~1.03 MPa (150 psi), limiting the maximum effective stress to ~0.75 MPa (110 psi). The sample was allowed to equilibrate for at least 4 hr and generally overnight. Once the target effective stress was achieved, cell pressure and backpressure were maintained. Vertical sample displacement and cell fluid volume were monitored throughout testing.

After the target effective stress level was achieved, a brief constant gradient test was conducted to select an appropriate flow rate for the subsequent constant flow tests. During the constant flow tests, flow rates were maintained by two pumps, one on each end of the sample, ensuring that the volume of the sample remained unchanged. Throughout the permeation step, the head gradient was monitored to assure that gradients were not excessive (ASTM, 1990). Since fluid pressure in the closed hydraulic system is sensitive to temperature changes, testing was conducted within a closed cabinet with a fan to keep the internal temperature uniform. This kept temperature at ~27.5°C (±0.5°C). Temperature was monitored throughout the testing phase.

Two to three constant flow tests were performed at each effective stress. Once permeability values were obtained, cell pressure was increased and the sample was allowed to equilibrate overnight. At least two different effective stress steps were performed for each sample. If the permeability of the sample decreased significantly from step 1 to step 2 during permeation, more steps were performed. The maximum effective stresses reached in this study are well below in situ values. Therefore, we used the permeability results from the highest effective stress, and the values presented in this study should be considered maximum permeability values. However, in previous laboratory investigations (e.g., Bolton and Maltman, 1998; Bolton et al., 2000), it appeared that the largest decrease in permeability occurred as effective stresses were increased from 0 to 0.1 MPa; subsequently, permeabilities remained relatively constant.

Measurements were made of the sample's diameter and height before it was placed in the cell. Using these measurements, the specified flow rate (Q), and the pressure difference that was monitored by the testing equipment, hydraulic conductivity values were calculated for each sample using Darcy's Law:

$$Q = -K \times A \times (dh/dl), \quad (1)$$

where

- K = hydraulic conductivity (in meters per second),
- A = the area of the sample (in square meters),
- dh = the difference in head across the sample (in meters), and
- dl = the length of the sample (in meters).

These conductivity values were then converted to permeability (in square meters) using the following equation:

$$k = (K \times \mu) / (\rho \times g), \quad (2)$$

where

- μ = viscosity (in pascal seconds),

ρ = density (in kilograms per cubic meter), and
 g = the gravitational constant.

A viscosity of 0.001 Pa·s was used for this calculation.

Numerical Modeling

Numerical modeling focused on Site 1108 to assess whether elevated pore pressures due to sedimentation are likely at the depth of the low-angle normal fault. Previous researchers (Gibson, 1958; Bredehoeft and Hanshaw, 1968) developed analytical models for this problem of estimating fluid pressures due to sedimentation. However, to model varying sediment rates and changes in storage properties through time, we used a one-dimensional numerical approach. This numerical approach was previously described by Sreaton and Ge (2000), but the calculation of compressibility within the model has been improved.

In the absence of overpressures, we assume that porosity will decrease exponentially with depth, as has been observed by Athy (1930):

$$n = n_0 \exp(-b \times z), \quad (3)$$

where

n = porosity,
 n_0 = initial porosity,
 b = a constant (in 1/meter), and
 z = burial depth (in meters).

For the hydrostatic case, the change in effective stress, σ_e , with depth is:

$$(d\sigma_e/dz) = (\rho_s - \rho_f) \times (1 - n) \times g, \quad (4)$$

where

ρ_s = grain density,
 ρ_f = fluid density, and
 g = the gravitational constant.

From Equations 3 and 4, dn can be related to $d\sigma_e$:

$$(dn/d\sigma_e) = (-b \times n) / [(\rho_s - \rho_f) \times (1 - n) \times g]. \quad (5)$$

The coefficient of vertical compressibility (α) is defined as

$$\alpha = -dV / (V \times d\sigma_e), \quad (6)$$

where

dV = the volume change (in cubic meters) and
 V = the volume (in cubic meters).

Porosity is related to the volume change by

$$dn = (1 - n) \times (dV/V). \quad (7)$$

The expression for α as a function of n follows from Equations 5, 6, and 7:

$$\alpha = (b \times n) / [(\rho_s - \rho_f) \times (1 - n)^2 \times g]. \quad (8)$$

The sedimentation history was broken up into packets for which sedimentation rate, porosity parameters n_0 and b , and permeability were assigned. The permeability remained constant for each packet throughout the simulation. Based on the sedimentation rate for each of the packets, the loading program calculated the additional thickness of each sediment layer added to the basin. As each new sediment layer was added to the basin, the layers beneath were moved down one row. Below the sediment layers, model layers were assigned low compressibility and porosities to simulate underlying crystalline rock. The bottom boundary condition of the model was no-flow and the top boundary condition was hydrostatic. The model was set up so that only nonsediment layers would be dropped from the bottom of the model.

For each sedimentation step, the pore fluid pressures of each layer were calculated based on the additional load of the new layers. When a porous medium with incompressible grains is loaded, the stress is partitioned between the pore fluid and the matrix. The loading efficiency, γ , denotes the fraction of the stress added to the pore fluid and is defined as follows (after Neuzil, 1986):

$$\gamma = \alpha / (\alpha + n\beta), \quad (9)$$

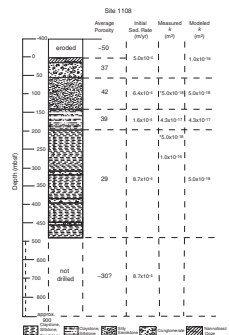
where β = the compressibility of the fluid. For highly compressible sediments, the loading efficiency is near 1.

The updated pore pressures were then input into SUTRA (Voss, 1984), which used the pore pressures as initial conditions for transient fluid flow for the duration of the sedimentation step. Once the pore pressures at the end of the sedimentation step were calculated in SUTRA, they were transferred back into the loading program and effective stress was calculated. Sediment porosity loss was calculated only if the effective stress exceeded the previous maximum effective stress value. Porosity loss was determined using a value from the previous sedimentation step and vertical node spacing was reduced to maintain constant solid volume and to ensure mass balance, while horizontal dimensions were held constant. The new porosity was used to calculate α for the next time step using Equation 8. The calculated compressibility was also used to assign specific storage, S_s , for each node to be used in the SUTRA fluid flow simulation:

$$S_s = \rho \times g \times (\alpha + n\beta). \quad (10)$$

Site 1108 was modeled to a depth of ~900 mbsf, the estimated depth of the low-angle normal fault zone. Values for the parameters n_0 (= 70%) and b (= $1.6 \times 10^{-3} \text{ m}^{-1}$) in Equation 3 were selected based on the porosity data from shallow parts of Site 1108, with the assumption that shallow depths are least likely to be overpressured. The sediment column of Site 1108 was broken down into five sediment packets (Fig. F2). The initial thickness of each packet was calculated based on ages, porosities, and depths reported shipboard and assumed an initial poros-

F2. Average porosities, sedimentation rates, and permeabilities, p. 13.



ity of 70% and conservation of solid volume. The top packet includes the 400 m that is inferred to have been removed by erosion. For the removed section, an average porosity of 50% was used. The sedimentation rate below the bottom of drilling (485 mbsf) was assumed to be the same as the overlying section, yielding an age at the bottom of ~4.4 Ma. The modeling was broken up into 75 sedimentation steps of 58.7 k.y. each.

RESULTS

Constant Flow Permeability Testing

Table T1 summarizes the permeability data for each sample, including the best estimate of permeability for each sample and the corresponding depths and porosities. Porosities were obtained from the shipboard data (Shipboard Scientific Party, 1999) and are not corrected for sediment rebound. The highest permeability at Site 1108, 1.0×10^{-16} m², was noted in Sample 180-1108B-30R-6, 32–52 cm, a silty sand from a depth of 280 mbsf. Site 1108 samples from Bolton et al. (2000) at depths of 121 and 218 mbsf yielded permeabilities of $\sim 5 \times 10^{-18}$ m². At Site 1115, permeability values from four samples ranged from 1.5×10^{-18} to 9.2×10^{-17} m². Results from four samples from Site 1118 yielded permeability values ranging from 8.6×10^{-18} to 5.9×10^{-17} m². No clear relationship between porosity and permeability is observed.

T1. Permeability results, p. 14.

Numerical Modeling

Permeabilities for the numerical model were based on results of the constant flow-rate tests (Fig. F2). For the section that was removed by erosion, a permeability of 1×10^{-16} m² was used. Because the sample from 280 mbsf was from a permeable layer of silty sand, it was assumed not to be representative of the overall vertical permeability of that sediment packet. Numerical modeling was used to constrain the permeabilities of the undrilled section (485–900 mbsf) necessary to create overpressures. We could then assess whether these permeabilities were probable and, thus, whether overpressures resulting from sedimentation were likely.

Overpressures are presented in terms of the excess pore pressure ratio, γ^* :

$$\lambda^* = (P_f - P_h) / (P_l - P_h), \quad (11)$$

where

- P_f = pore fluid pressure,
- P_h = hydrostatic pressure, and
- P_l = lithostatic pressure, the weight of the sediment column.

At Site 1108, slight overpressures ($\lambda^* > 0.1$) initiate at $k = 3.4 \times 10^{-19}$ m² for the missing section. For significant overpressures ($\lambda^* > 0.7$) to occur at the base of the sediment column, the permeability of the missing sediment would have to be 2.0×10^{-19} m² or less. Results are not very sensitive to uncertainties in the sedimentation rate of the undrilled section. With the sedimentation rate of the section from 485 to 900 mbsf dou-

bled, slight overpressures ($\lambda^* > 0.1$) initiate at $k = 4.2 \times 10^{-19} \text{ m}^2$ for the missing section.

DISCUSSION

Results from one-dimensional modeling of Site 1108 suggest that overpressures due to sedimentation require permeabilities less than $3.4 \times 10^{-19} \text{ m}^2$. Although permeability values in that range would be reasonable for clay-rich sediments (Neuzil, 1994), sediments in Woodlark Basin have a greater component of medium- to coarse-grained material. The lowest permeability measured at Site 1108 was $5.0 \times 10^{-18} \text{ m}^2$, whereas the lowest overall permeability measured during this investigation was $1.5 \times 10^{-18} \text{ m}^2$. The low value was measured for Site 1115 sediments at 678 mbsf. Therefore, it does not seem likely that permeabilities below Site 1108 are lower than $3.4 \times 10^{-19} \text{ m}^2$, although it is possible that extensive cementation could cause low permeability in the base of the rift basin.

The modeling assessed only overpressures due to one-dimensional loading. Additional pressure-generating mechanisms, such as hydrocarbon generation, clay dehydration, or additional input of fluids from greater depths of the fault zone are likely to be active in Woodlark Basin. The high thermal gradient in this area ($\sim 94\text{--}100^\circ\text{C}/\text{km}$) (Shipboard Scientific Party, 1999) would put the base of the section in the range for smectite dehydration.

On the other hand, overpressures could be reduced by escape of fluids along lateral conduits or fault zones. The occurrence of sand layers may provide lateral conduits for fluid flow within the basin. For example, Sample 180-1108B-30R-6, 32–52 cm, at 280 mbsf, yielded permeability values of $1.0 \times 10^{-16} \text{ m}^2$, 20 times greater than those reported for Site 1108 samples from 121 and 218 mbsf (Bolton et al., 2000). Temperatures observed during logging of Site 1118, at the margin of the rift basin, suggested the occurrence of a thermal anomaly at depth, which may be an indication of lateral and upward fluid migration from the basin (Shipboard Scientific Party, 1999). Lateral fluid migration could lower pressures within the basin and transfer overpressures to the basin margins.

SUMMARY

Constant-rate flow tests were conducted on 10 cores from Sites 1108, 1115, and 1118. Results of the laboratory tests indicated permeabilities that range from 1.5×10^{-18} to $5 \times 10^{-16} \text{ m}^2$. The permeability data, as well as data from other researchers, were used to assign permeabilities to model overpressures at the base of Site 1108. Results of one-dimensional modeling suggest that overpressures resulting from sedimentation initiate when permeabilities of the base sections are less than $3.4 \times 10^{-19} \text{ m}^2$ and reach near-lithostatic values if the average permeability of the base is less than $2.0 \times 10^{-19} \text{ m}^2$. The available data provide no indication of permeabilities in that range. Therefore, overpressures due to sedimentation alone are considered unlikely.

ACKNOWLEDGMENTS

The authors would like to thank the crew of the *JOIDES Resolution* and the ODP Leg 180 scientific team, especially S. Stover, for help collecting the samples. Detailed reviews by Pierre Henry and Demian Saffer improved the manuscript. Financial support was provided by a JOI/USSSP grant to E. Sreaton and National Science Foundation Grant OCE-9811293 to E. Sreaton.

REFERENCES

- ASTM, 1990. Standard test method for measurement of hydraulic conductivity of saturated porous materials using a flexible wall permeameter. Philadelphia (Am. Soc. Test. Mater.), D5084.
- Athy, L.F., 1930. Density, porosity, and compaction of sedimentary rocks. *AAPG Bull.*, 14:1–24.
- Axen, G.J., 1992. Pore pressure, stress increase, and fault weakening in low-angle normal faulting. *J. Geophys. Res.*, 97:8979–8991.
- Bethke, C.M., 1985. A numerical model of compaction-driven groundwater flow and heat transfer and its applications to the paleohydrology of intracratonic sedimentary basins. *J. Geophys. Res.*, 90:6817–6828.
- Bjørlykke, K., and Hoeg, K., 1997. Effects of burial diagenesis on stresses, compaction and fluid flow in sedimentary basins. *Mar. Pet. Geol.*, 14:267–276.
- Bolton, A., and Maltman, A., 1998. Fluid-flow pathways in actively deforming sediments: the role of pore fluid pressure and volume change. *Mar. Pet. Geol.*, 15:281–297.
- Bolton, A., Maltman, A.J., and Fisher, Q., 2000. Anisotropic permeability and bimodal pore-size distributions of fine-grained marine sediments. *Mar. Pet. Geol.*, 17:657–672.
- Bredehoeft, J.D., and Hanshaw, B.B., 1968. On the maintenance of anomalous fluid pressures: 1. Thick sedimentary sequences. *Geol. Soc. Am. Bull.*, 79:1097–1106.
- Bredehoeft, J.D., Djevanshir, R.D., and Belitz, K.R., 1988. Lateral fluid flow in a compacting sand-shale sequence: South Caspian Basin. *AAPG Bull.*, 72:416–424.
- Gibson, R.E., 1958. The progress of consolidation in a clay layer increasing in thickness with time. *Geotechnique*, 8:71–182.
- Hubbert, M.K., and Rubey, W.W., 1959. Role of fluid pressures in mechanics of overthrust faulting, Part 1. Mechanics of fluid-filled porous solids and its application to overthrust faulting. *Geol. Soc. Am. Bull.*, 70:115–166.
- Mello, U.T., and Karner, G.D., 1996. Development of sediment overpressure and its effect on thermal maturation: Application to the Gulf of Mexico Basin. *AAPG Bull.* 80:1367–1396.
- Mobbs, K., 1997. Tectonic interpretation of the Papua New Guinea region from repeat satellite measurements [M.S. Thesis]. Univ. South Wales.
- Neuzil, C.E., 1986. Groundwater flow in low permeability environments. *Water Resour. Res.*, 22:1163–1195.
- , 1994. How permeable are clays and shales? *Water Resour. Res.*, 30:145–150.
- Osborne, M.J., and Swarbrick, R.E., 1997. Mechanisms for generating overpressures in sedimentary basins: a reevaluation. *AAPG Bull.*: 81:1023–1041.
- Person, M., and Garven, G., 1994. A sensitivity study of the driving forces on fluid flow during continental-rift basin evolution. *Geol. Sci. Am. Bull.*, 106:461–475.
- Person, M., Raffensperger, J.P., Ge, S., and Garven, G., 1996. Basin-scale hydrogeologic modeling. *Rev. Geophys.*, 34:61–87.
- Rice, J.R., 1992. Fault stress states, pore pressure distributions, and the weakness of the San Andreas fault. In Evans, B., and Wong, T.-F. (Eds.), *Fault Mechanics and Transport Properties of Rocks: a Festschrift in Honor of W. F. Brace*: San Diego (Academic Press), 475–503.
- Screaton, E.J., and Ge, S., 2000. Anomalously high porosities in the proto-decollement zone of the Barbados accretionary complex: do they indicate overpressures? *Geophys. Res. Lett.*, 27:1993–1996.
- Shipboard Scientific Party, 1999. Leg 180 summary. In Taylor, B., Huchon, P., Klaus, A., et al., *Proc. ODP, Init. Repts.*, 180: College Station, TX (Ocean Drilling Program), 1–77.
- Taylor, B., Goodliffe, A., Martinez, F., and Hey, R., 1995. Continental rifting and initial sea-floor spreading in the Woodlark Basin. *Nature*, 374:534–537.

Voss, C.I., 1984. A finite element simulation model for saturated-unsaturated, fluid-density-dependent groundwater flow with energy transport or chemically-reactive single-species solute transport. *U.S. Geol. Surv. Water-Resour. Invest.*, 84-4369:409.

Figure F1. Location of Sites 1108, 1109, 1115, and 1118 relative to Moresby Seamount.

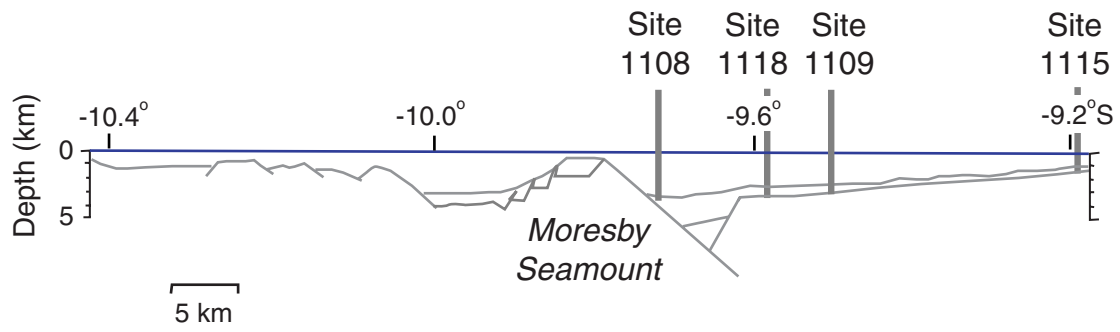


Figure F2. Average porosities, initial sedimentation rates, and permeabilities used for modeling of Site 808.
 * = data from Bolton et al. (2000).

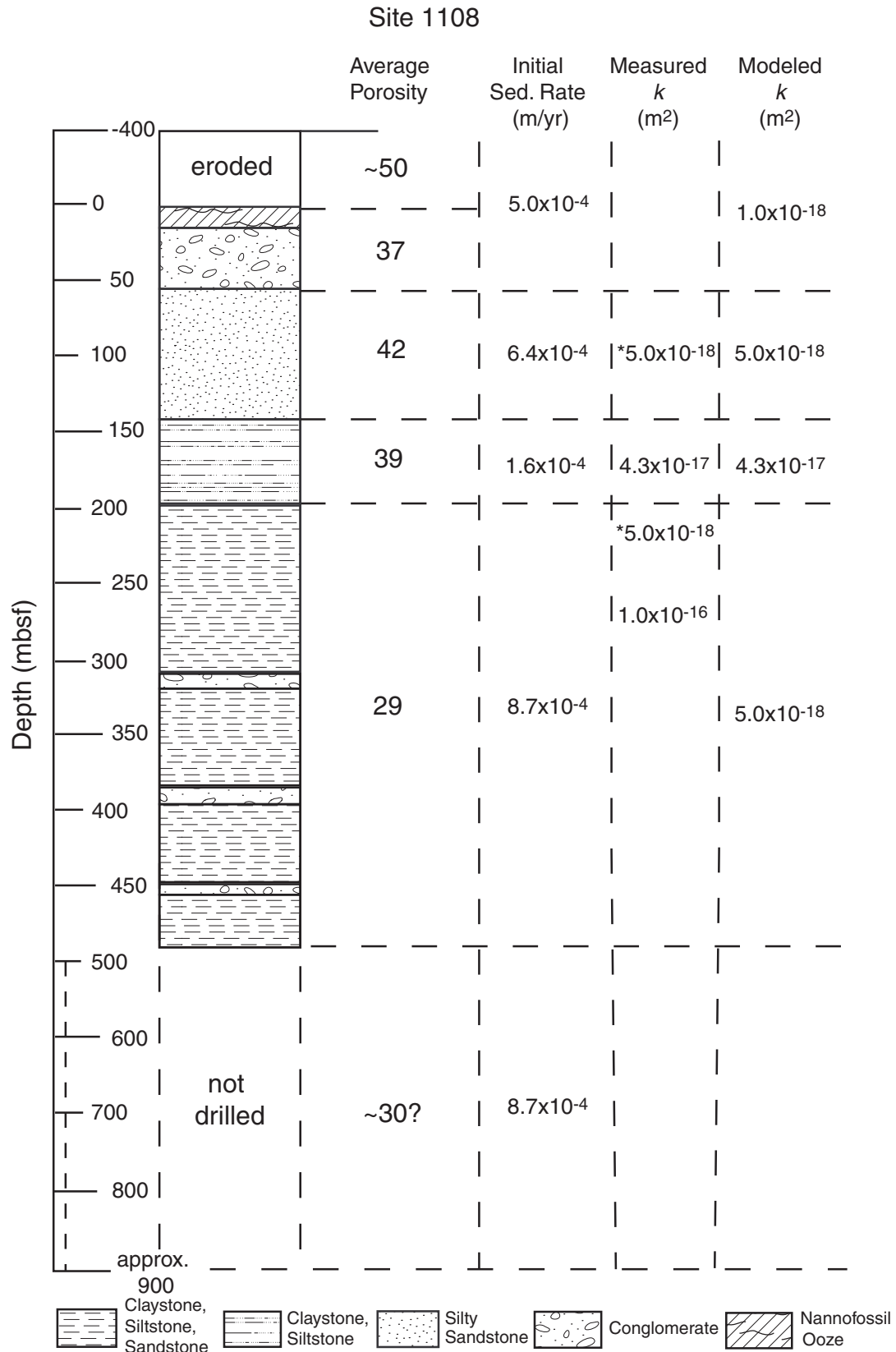


Table T1. Summary of permeability results.

Core, section, interval (cm)	Depth (mbsf)	Porosity (%)	Estimated permeability (m ²)
180-1108B-			
21R-1, 134-147	188	35.1	4.3×10^{-17}
30R-6, 32-52	280	28.5	1.0×10^{-16}
180-1115C-			
12R-3, 0-20	392	57.1	3.6×10^{-17}
22R-2, 56-76	487	49.2	3.7×10^{-17}
30R-1, 34-53	561	41.8	9.2×10^{-17}
42R-1, 64-79	678	38.4	1.5×10^{-18}
180-1118A-			
25R-3, 110-123	439	46.3	5.9×10^{-17}
45R-5, 56-73	633	46.6	4.7×10^{-17}
180-1118C-			
56R-3, 56-76	487	49.2	3.7×10^{-17}
180-1118A-			
63R-4, 72-93	737	50.2	8.6×10^{-18}